Kinetic and mechanistic analysis of membrane fouling in microplastics removal from water by dead-end microfiltration

A. Raffaella P. Pizzichetti [a,b], Cristina Pablos [a,*], Carmen Álvarez-Fernández [a], Ken Reynolds [b], Simon Stanley [b], Javier Marugán [a]

[a] Department of Chemical and Environmental Technology, ESCET, Universidad Rey Juan Carlos, C/Tulipán s/n, Móstoles, Madrid 28933, Spain
[b] ProPhotonix IRL LTD, 3020 Euro Business Park, Little Island, Cork T45 X211, Ireland

ARTICLE INFO

ABSTRACT

This study explores and analyses the kinetic and mechanistic aspects of microfiltration cellulose acetate membrane fouling by polyamide (PA) and polystyrene (PS) particles in dead-end configuration and the main interactions between the microplastics and the membrane during the filtration process. First, PA and PS particles were characterised to define the differences in shape (regular and irregular), particle size distribution (10–105 μm and 20–320 μm), and surface charge (neutral and negative). The results showed that the prevailing mechanisms during microplastic filtrations were complete pore blocking followed by cake layer formation in both cases. The mechanisms' kinetics were positively correlated to MPs load through a power-law relationship which was stronger for PS than for PA particles because of higher steric hindrance effects. On the other hand, increasing the working transmembrane pressure led to an optimum working condition, between 0.3 and 0.5 bar for PA and 0.3 bar for PS filtration. Overall, higher fouling was induced by the PA particles due to the higher PA hydrophobicity and their smaller size, which caused a denser cake layer. Instead, PS particles with higher irregularities and repulsive electrostatic forces formed a more porous layer but induced a high degree of abrasion on the membrane surface. Finally, membrane fouling led to an increase in hydrophobicity and roughness, probably causing further fouling. To conclude, modelling membrane fouling can help predict the best working conditions and the membrane replacement cycles to increase the MPs removal efficiency and reduce secondary MP-based pollution.

1. Introduction

Water is an essential resource for life, and providing safe drinking water is essential in both industrialised and developing countries. Recently, water safety has been at risk due to the release of newer uncontrolled pollutants known as contaminants of emerging concerns

(CECs) [1,2]. Nowadays, within the CECs, microplastics (MPs), defined as plastic particles below 5 mm in size, are growing a significant interest considering their ubiquitous presence worldwide [3]. Plastic products have intensively increased in the last decades, and in 2019, global plastic production almost reached 370 million tonnes [4]. Plastic is a versatile material with many useful properties (e.g., flexibility, strength, durability, and low price) that suit many applications; therefore, practically unavoidable in modern life. However, its abuse and improper waste disposal have led to its widespread presence in the environment [5]. In addition, plastic is resistant to biodegradation, increasing the risk of accumulation on land and water bodies [6]. The sources of MPs are many, among them, fragmentation of plastics due to the photo, mechanical, and microbial effects (categorised as secondary microplastics) and polymer particles manufactured smaller than 5 mm for specific add-ons in textiles, medicines, and personal care products, such as skin exfoliators and shower gels (categorised as primary microplastics) [7,8]. Wastewater treatment plants (WWTPs) also play an important role in releasing them into the environment, producing artificial stresses and inducing fragmentation of larger plastic particles before discharging them into nature [7,9].

The threat to the marine ecosystem has already been extensively reported [10–13]. The omnipresence of MPs in water is causing symptoms in aquatic animals, such as malnutrition, inflammation, chemical poisoning, oesophagus blockage, abnormal growth, and a decrease in fecundity. Also, as plastics are highly stable, they accumulate in the bodies and cause long-term damage and, lastly, death. The toxicity may result from the leaching of plastic additives, such as flame retardants, endocrine disruptors, phthalates, and further emerging toxic contaminants [14,15]. It is also well known that they attract on their surface other persistent organic pollutants (POPs), among them dichlorodiphenyltrichloroethane (DDT), polychlorinated biphenyls (PCBs), and other dioxin-like chemicals [15–17]. Finally, they act as a vector of pharmaceuticals, promoting their bioaccumulation and biomagnification through the food chain [18,19], and pathogens, leading to a dispersion of species in new ecosystems [20]. The potential threats of MPs to human health led to further investigations into other human-related food and environments, and their presence has been detected in drinking water, bottled water, beer, table salt, honey, seafood, and even in the air [21–23]. MPs enter the food web at different trophic levels and then transfer bottom-up along all the levels.

Despite a reasonable degree of removal, a significant amount of MPs are still discharged by WWTPs and drinking water treatment plants (DWTPs) [24]. For example, in a study conducted on several wastewater treatment facilities' effluents in the US, Mason et al. [25] estimated that over 4 million microplastic particles were released daily per facility. Nevertheless, no legislative law limits MPs' contamination in drinking water, but until now, some attention has been paid to their removal [25, 26]. However, considering the different routes of MPs to freshwater, many efforts to improve water quality should be made directly at the drinking water level [27].

Among the main engineered technologies explored for MPs removal [28–33], such as electrocoagulation [34], magnetic extraction [35,36], electrostatic separation [37], biological digestion and degradation [38, 39], UV irradiation [40,41], ozonation [42–44], and Fenton-like reactions [28,45] (summarised in Appendix A of the Supplementary Information), membranes captured significant attention combined or not with coagulation/flocculation processes [46,47] or agglomeration reactions induced by sol-gel (alkoxy-silyl) [48]. Membrane technology can play a fundamental role in tackling the problem of MPs [49]. It has already been extensively used for advanced drinking water treatments, and, depending on the membrane pore size and the material, it can be specific to intercept different pollutants. Furthermore, it has several advantages, such as simple operation, good selectivity, low energy consumption, and stable effluent quality. By now, several membrane processes have been explored for microplastic removal, such as micro (MF), ultra (UF) and nano-filtration (NF), reverse osmosis (RO),

membrane bioreactor (MBR), and dynamic membrane (DM) [50]. Despite extensive studies performed on microplastic filtration, there is very little research focused on the membrane fouling behaviour by microplastics [51–54]. Nonetheless, fouling represents a critical problem for the design and operation of the system, and it needs to be investigated to develop more efficient solutions, identify effective cleaning strategies, and plan membrane replacement cycles. As a result of the significant knowledge gap, the need to investigate microplastics' impacts on the membrane surface and be able to predict the fouling degree under different working conditions to model the fouling scenario and design the system accordingly, with an eye to operational costs and environmental implications. Filling the gap would, in fact, encourage and allow the safe implementation of membrane systems in our daily water treatments, including in household systems.

Microfiltration was chosen since, together with dynamic membranes [55], it has the simplest implementation and the lowest operational energy costs compared to the other processes. Also, it can be directly employed in domestic and industrial systems without any further treatment. For the membrane material, cellulose acetate (CA) was chosen for its good performance and high mass and particle number removal efficiency [56], and among the MPs, polyamide (PA) and polystyrene (PS) were chosen since they were found in great percentages in different environments [7]. Two types of MPs were employed to assess the differences in the MPs chemistry and, consequently, changes in size distribution and shapes coming from distinct manufacturing processes. Finally, dead-end configuration and constant transmembrane pressure (TMP) were chosen for their easy implementation on a small scale; therefore, suitable for domestic environments or limited capacity DWTPs [57]. To the best of the authors' knowledge, this is the first study deeply analysing the membrane fouling impact by different microplastics, assessing the kinetic constants trend under different working conditions with the aim to evaluate optimal filtration settings other than identifying the major membrane surface impacts. A lab-scale filtration setup was designed, and the flow rate was monitored during the entire filtration run. Following a first characterisation of the MPs and the membrane, this study focuses on (1) identifying the main successive fouling mechanisms using Hermia's model equations; (2) quantifying the kinetic constants for each mechanism as a function of the suspension type (PA and PS) and the operating parameters, varying TMP (0.1, 0.3, 0.5, and 0.7 bar) and MPs load (1, 5, 10, and 20 mg/L); and (3) assessing the influence of the MPs characteristics on the membrane fouling.

2. Materials and methods

2.1. Materials

Polyamide nylon 6 and polystyrene microparticles were purchased from Goodfellow. The working particle range was selected between 20 and 300 μm to be a representative size in water bodies, but considering the detection limit of the micro-Fourier Transform Infrared Spectroscopy (micro-FTIR) equipment, down to 20 μm [3]. In the case of PA, all the particles were manufactured below 300 μm, while the PS particles bigger than 300 μm were first reduced by cryogenic milling (ZM 100, Retsch with stainless steel mortar material at a speed of 14000 rpm, and the temperature cooled down with liquid nitrogen). Then both particles were sieved between 20 and 300 μm. The sieves of 300 μm, 20 μm, and a sieve pan were purchased from Scharlab. Cellulose acetate (CA) membranes were purchased from Mervilab, with 47 mm diameter and nominal pore size of 5 μm, which was chosen to enhance the advantages of microfiltration while ensuring a good removal.

2.2. Characterisation techniques

2.2.1. Reflectance micro-FTIR and attenuate total reflection-FTIR

FTIR analyses were performed to characterise the chemical structure of the PA and PS particles directly on the membrane surface. Spectra

were obtained in reflectance from a PerkinElmer Spotlight 200i microscope coupled with the FTIR Frontier Spectrometer, in the wavelength range of 4000–600 cm^{-1} and at room temperature, with 8 cm^{-1} resolution and 30 scans. Attenuated total reflection (ATR)- FTIR spectra were obtained in the same wavelength range, resolution, and scans with a diamond crystal.

2.2.2. Microplastic particle size distribution

Particle size distribution of the MP suspensions were analysed through microscopic counting and focused beam reflectance measurement (FBRM). Microscopic counting consisted of taking pictures through an optical microscope (B3 Series, Motic) with an objective lens magnification of 10x and a camera attached to the lens (Moticam3 3.0 MP, Motic). The pictures were then processed with Image J Software. The second technique was performed by the FBRM M500LF Lasentec apparatus manufactured by Mettler Toledo. The instrument operates by scanning a laser beam at a fixed speed across the particles stirred in suspension. The particle crossing the beam reflects part of the light, and from the duration of the backscattered light, the instruments can measure the chord length distribution, which is the raw outcome [58]. Then, assuming a spherical shape of the particles, the model reported by Hukkanen and Braatz was used to convert the chord length distribution (CLD) into the particle size distribution (PSD) [59]. The model is based on probability functions constructed for each particle size vector, f, and the corresponding chord length vector, c, as shown in Eq. (1).

$$c = \mathbf{P_{ij}} \bullet f \tag{1}$$

The elements of the matrix P_{ij} are described by Eq. (2) when considering a midpoint distribution within the range D_j and D_{j+1}.

$$\mathbf{P_{ij}} = \begin{cases} \sqrt{1 - \left(\dfrac{2D_i}{D_j + D_{j+1}}\right)^2} - \sqrt{1 - \left(\dfrac{2D_{i+1}}{D_j + D_{j+1}}\right)^2} & i < j \\[2ex] \sqrt{1 - \left(\dfrac{2D_{i+1}}{D_j + D_{j+1}}\right)^2} & i = j \\[2ex] 0 & i > j \end{cases} \tag{2}$$

Where the jth column represents the chords distribution and the ith column the paxzrticle size distribution. Hence, the inverse matrix P_{ij}^{-1} allows the estimation of PSD from CLD. Finally, the Minitab Statistical Software was employed to identify the distribution fitting and its main parameters.

2.2.3. Scanning electron microscope

PA and PS particles' morphology was analysed using scanning electron microscopy (SEM - XL 30 ESEM, Philips) operating in the potential range of 5 kV at 5.8 and 5.4 mm working distance, respectively. Membrane surface and cross-section were also analysed at a working distance varying from 4.5 to 6.3 mm. Finally, images after MPs filtration were obtained using a JEOL JSM 7600 F Field Emission SEM at an accelerating voltage of 5 kV and 8–9 mm working distance.

2.2.4. Water contact angle (WCA)

Water contact angle (WCA) measurements were taken to evaluate the hydrophilicity on the membrane before and after the MPs filtration. It was carried out by the sessile drop technique (Ramé-Hart 200-F1). Distilled water droplets were deposited on the surface of the membrane, and macrographs of the droplets were taken at 10, 30, and 60 s after the deposition. Subsequently, the water contact angle was evaluated by an image analysis software using the goniometer function. At least three drops were measured for each sample.

2.2.5. Membrane roughness

A 3D optical profilometer (Zeta-20 Desktop Optical Profiler) was employed to measure the surface profile and roughness of the CA

membranes in comparison with other commercial membranes, polycarbonate and PTFE membranes, and before and after the MPs filtration. The results show an average of ten measures for each position, where at least three sites for each membrane were evaluated.

2.3. Filtration system

The filtration setup system is schematised in Fig. 1. It consisted of a glass container of 5 L with a bottom exit connected to a centrifugal pump (model TP 78/A, Calpeda) through a needle valve. The bottle was continuously stirred at 500 rpm (Agimatic-E, J.P. Selecta) to ensure homogeneity of the MPs distribution in water, and it was constantly filled with fresh MPs solution throughout the entire run. The pump was connected to a variable-frequency drive (VFD) (RS510, RS Pro) and controlled through an Arduino Mega 2560 board, integrated with a keypad, an LCD monitor, and current-to-voltage converters to work at the desired constant pressure. Temperature, pressure, and flow rate sensors are placed before the membrane filtration system. They were first connected to a data logger (Aplisens PMS-90R) for direct measurement and then used as input for the Arduino board to control the VFD and work at constant TMP. The Arduino code can be found in the GitHub repository. All the experiments were carried out at room temperature and with an operating pressure varying from 0.1 to 0.7 bar.

Distilled water from Milli-Q Direct-Q® 8 UV (Merck Millipore), with a neutral pH of around 6.5, was used in all the experiments to avoid other contamination and uncontrolled effects on the fouling mechanisms. Although it is known that MPs are not the only reason for severe fouling of membrane processes and other water constituents also play a significant role [53,60,61], the quality of water can change substantially with time and space, giving some unreliable data on the MPs contribution on membrane fouling. Therefore, by knowing their behaviour in pure water, it is easier to identify the main MPs-membrane interactions and address only the experimental variables (particle size and shape, hydrophobicity, charge, and roughness).

2.4. Modelling of the membrane fouling in dead-end filtrations at constant pressure

Four mechanistic models are generally used to describe fouling: cake filtration, the mechanism in which particles accumulate at the surface in a permeable cake of increasing thickness that adds a hydraulic resistance to filtration; complete pore blocking, which assumes a seal of pore entrance and prevention of any flow through them; intermediate or partial pore blocking, a seal of pore entrance by a fraction of particles and a deposition of other particles on top of it; and standard or internal pore blocking, which assumes an accumulation inside the membrane on the pore walls and reduce the membrane permeability.

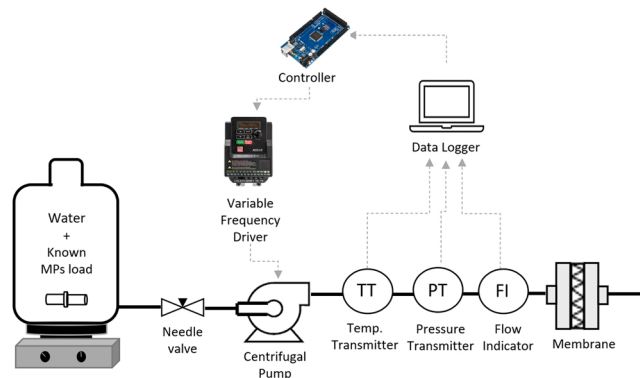For dead-end filtration working at constant pressure, fouling mech-

Fig. 1. Filtration system used in the laboratory to evaluate cellulose acetate membrane fouling by MPs.

anistic models have been developed based on Hermia's equation, Eq. (3) [62,63].

$$\frac{d^2t}{dv^2} = K_n \left(\frac{dt}{dv}\right)^n \tag{3}$$

Where v is the volume of filtrate per effective membrane area collected in time t, n depends on the filtration mechanism involved, and K_n is the specific constant for the mechanism n. Hermia's blocking law defines the changing rate in the filtration resistance, $d(dt/dv)/dv$, proportional to the filtration resistance, dt/dv, raised to a power n, which depends on the filtration mode [57].

However, as analyses of membrane filtration are normally performed in terms of flux decline over time, Eq. (3) can be rewritten in a physically more meaningful form where the filtration rate "$J=dv/dt$" is used to represent the blocking filtration law, Eq. (4) [64]. (Additional mathematical details can be found in Appendix B of the Supplementary Information).

$$\frac{dJ}{dt} = -K_n J^{3-n} \tag{4}$$

Finally, Table 1 summarises the equations for all four mechanisms.

Previous studies have highlighted three main cases depending on the diameter size of the membrane pores (d_{pore}) and the particles ($d_{particle}$) [51,65–67], as described in Table 2.

Furthermore, according to Grenier et al. [65], the kinetic constants of complete pore blocking and cake filtration are correlated respectively with the parameters η_B, blocked surface area by unit of time and surface of the membrane, and η_C, the volumic specific resistance of the cake. Their correlation has been modelled starting with the Darcy law equation, Eq. (9):

$$J = \frac{\Delta P}{\mu R} = \frac{\Delta P}{\mu(R_m + R_C)} \tag{9}$$

where R_m is the hydraulic resistance of the membrane and R_C is the hydraulic resistance of the cake.

In turn, the membrane hydraulic resistance also depends on the complete pore blocking mechanism, $R_{m,B}$, accordingly to Eq. (10).

$$R_{m,B} = \frac{R_{m,0}}{1 - \eta_B(V/A_0)} \tag{10}$$

Where $R_{m,0}$ is the clean membrane hydraulic resistance and η_B is correlated to the kinetic constant K_b as described by Eq. (11).

$$\eta_B = \frac{K_b}{J_0} \tag{11}$$

While the cake hydraulic resistance depends on η_C in agreement with Eq. (12), and the correlation to the kinetic constant K_c is described by Eq. (13).

$$R_C = \frac{\eta_C}{A_0} \bullet V \tag{12}$$

Table 1
Fouling mechanisms for constant pressure filtrations.

Fouling mechanism	n	K_n	Flux equation	Eq. (#)
Complete pore blocking	2	K_b	$J = J_0 e^{(-K_b t)}$	(5)
Internal or Standard pore blocking	1.5	K_s	$J = J_0 \bullet \left(1 + \frac{K_s J_0^{0.5} t}{2}\right)^{-2}$	(6)
Partial or Intermediate pore blocking	1	K_i	$J = J_0 \bullet (1 + K_i J_0 t)^{-1}$	(7)
Cake filtration	0	K_c	$J = J_0 \bullet \left(1 + 2K_c J_0^2 t\right)^{-\frac{1}{2}}$	(8)

Table 2
Effect of particle diameter versus membrane pore diameter.

Case	Main Mechanisms
$d_{pore} > d_{particle}$	Internal pore blocking, followed by the other mechanisms once the pores reduce in size
$d_{pore} \leq d_{particle}$	Pore blocking (complete and intermediate), followed by cake filtration
$d_{pore} \ll d_{particle}$	Cake filtration

$$\eta_C = \frac{\Delta P \bullet K_c}{\mu} \tag{13}$$

3. Results and discussion

3.1. Characterisation results

3.1.1. Micro-FTIR

To date, the analysis of MPs pollution in water is still one of the main challenges related to their occurrence since the microparticles can be easily confused with other materials [25]. Within the MP characterisation techniques, micro-FTIR has gained a lot of attention as suitable for both quantification and qualification. In fact, it is able to identify the plastic particles visually and by the determination of their chemical structure [68–70]. It is highly reliable and is non-destructive with minimal need for sample preparation, as it can be used to directly measure on the membrane filter by performing a "chemical mapping". However, previous studies have shown that refractive error represents a source of uncertainty when interpreting the spectra of irregularly shaped materials [69]. Consequently, to help the identification of CA, PA and PS micro-FTIR spectra, they were compared to their respective ATR-FTIR spectra, Fig. 2. Microplastics' identification is based on their key characteristic peaks evident in the ATR-FTIR spectra, where the main two regions are 3300–2700 cm^{-1} (for N-H stretch and C-H stretch) and 1800–1300 cm^{-1} (for C=O stretch, N-H bend, and C-C stretch) [71], identified in Fig. 2c by the black dash-dotted lines and the dotted lines respectively.

Although the spectra distortion caused by the refractive errors is noticeable and the baseline fluctuation quite large, the absorbance regions related to the main stretching and bending bonds are present for both microplastics, as shown in Fig. 2c, contrary to a previous study where the spectrum of polyamide nylon-6 was unattainable in reflectance micro-FTIR [68]. These results show that micro-FTIR is suitable for MPs identification directly on the cellulose acetate membrane, and its use can be extended in other works with more complex matrixes. However, the main drawback is the detection limit down to 20 μm size. Consequently, other techniques, such as Raman spectroscopy, should be employed to examine smaller size particles [3,72].

3.1.2. Particle Size Distribution

The particle size distribution is shown in Fig. 3a and Fig. 3b, for PA and PS particles, respectively, measured by microscopic counting (the histograms) and FBRM technology (the black curves).

The results from the two techniques are comparable, showing for PA an average value of around 40 μm (41 ± 16 μm and 39 ± 29 μm from microscopic and FBRM, respectively), while for PS particles an average value of around 110 μm (109 ± 74 μm and 109 ± 70 μm from microscopic and FBRM, respectively). Since both particle size distributions were right skewed, the histogram data were fitted to a Log-Normal distribution, represented in Fig. 3 by the short-dash dot curve in green. The Log-Normal distribution main parameters, location and scale, were 3.65 and 0.39 for PA, and 4.60 and 0.81 for PS, while the mean values were respectively 41 μm and 138 μm. Despite the particles being sieved in the range of interest of 20–300 μm, particles smaller in size could agglomerate with each other and particles greater in size could pass through the 300 μm sieve thanks to the shortest side of their
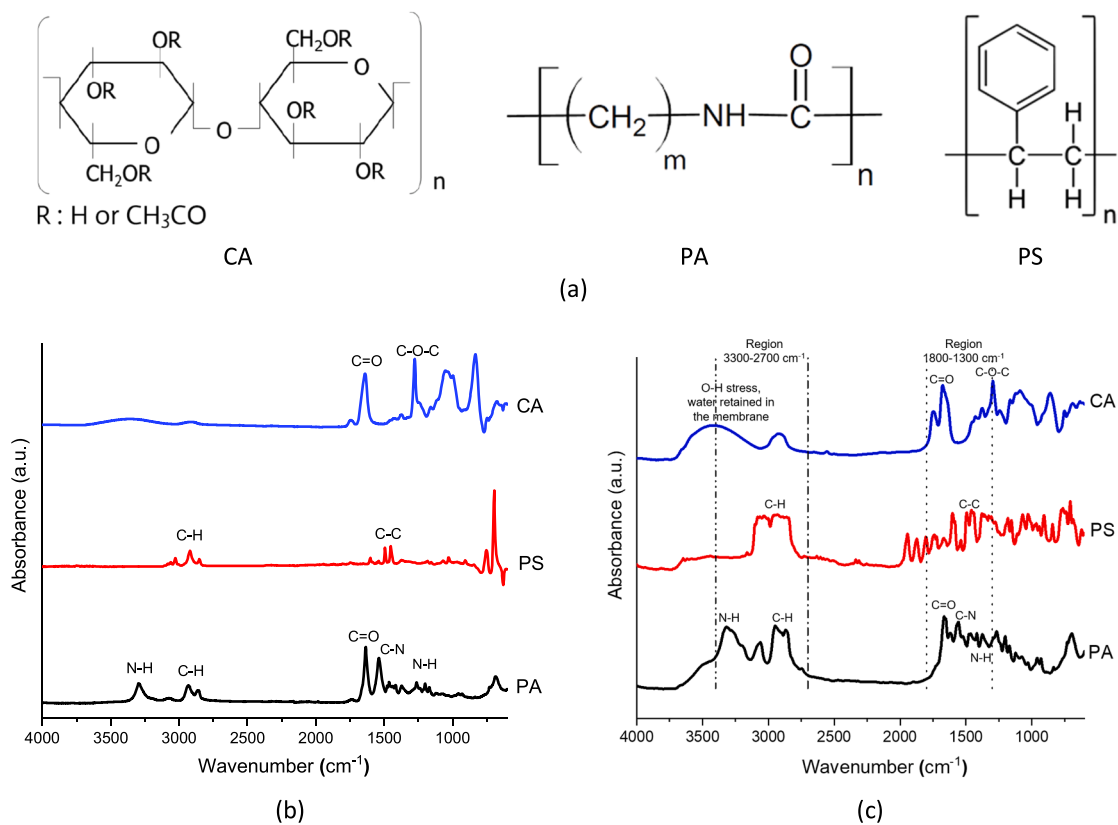
Fig. 2. Chemical structure of CA, PA, and PS (a), ATR-spectra (b), reflectance micro-FTIR spectra (c).
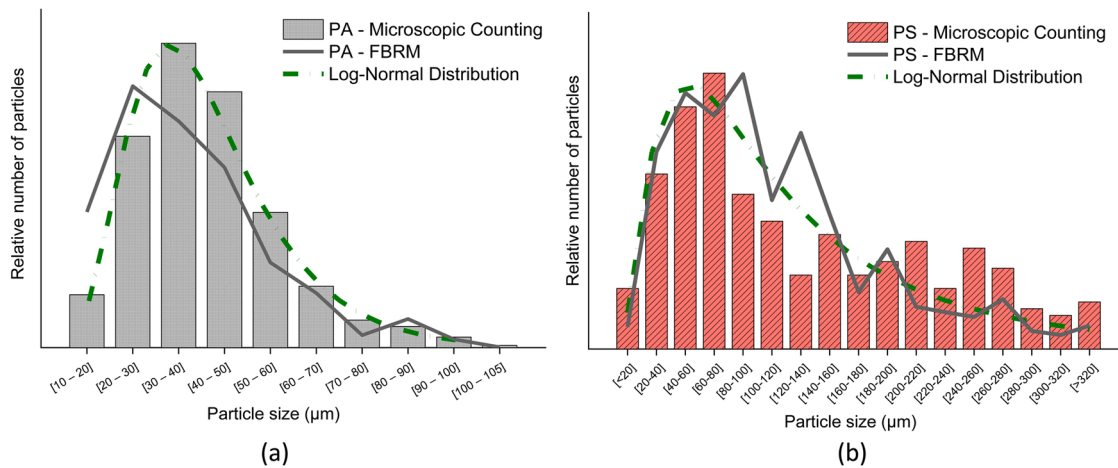

Fig. 3. Particle size distribution of polyamide nylon 6 (a) and polystyrene particles (b) after being milled and sieved in the range of 20–300 μm measured by microscopic counting (the histograms) and FBRM technology (the black curve). The short-dash dot curve in green represents the Log-Normal distribution fitting the histogram data.

irregular shape.

3.1.3. Scanning Electron Microscope

The SEM images of the microplastics are shown in Fig. 4 and highlight the difference in shape irregularities between the synthesised PA particles and the milled PS fragments. To notice that the images were taken at different magnifications to allow a similar representation of the particles, 2400x and 8000x in Fig. 4a and b, and 300x and 1200x in Fig. 4c and d. Different MP types in the environment often have different morphologies considering their diverse purpose in the market or the route by which they get into the water bodies. Although the results will

not be able to assess the predominant fouling factor among the MPs variables, which is out of the scope of this study, they help to identify how they impact the membrane surface. In this case, it can also be argued that they represent differences between primary MPs, directly produced as microbeads, and secondary microplastics, derived from macroplastic fragmentation.

SEM images of the commercial cellulose acetate membrane were also taken and shown in Fig. 5 to study the morphology and the pore distribution of the membrane employed. The membranes have a thin dense layer of smaller pore size to make the material selective without impacting the permeation flux, and under it, a highly porous structure
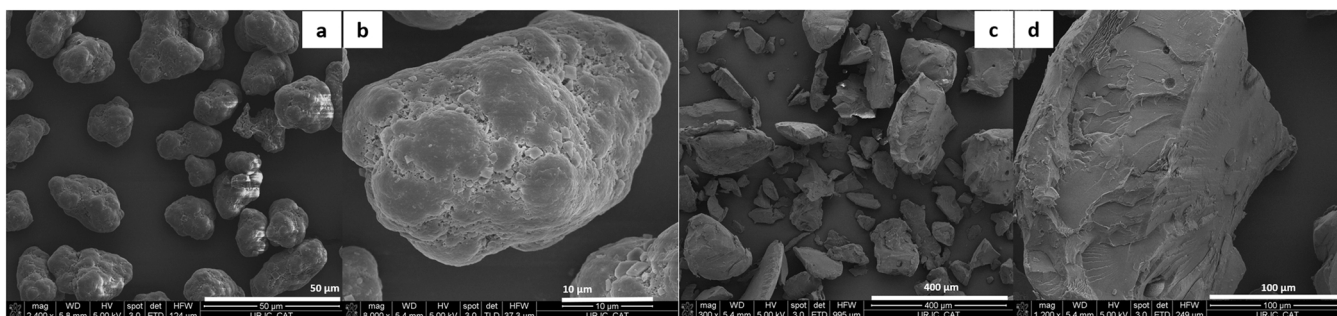
Fig. 4. SEM images of the particles of PA (a and b with unit distance of 50 and 10 μm) and PS (c and d with unit distance of 400 and 100 μm).
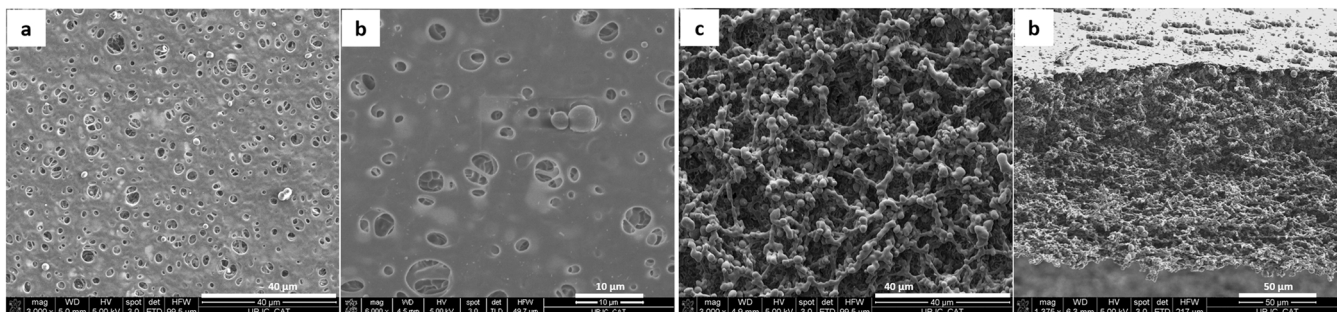

Fig. 5. SEM images of the membrane surface, up-face (a and b with unit distance of 40 and 10 μm), down-face (c with unit distance of 40 μm), and cross-section (d with unit distance of 50 μm).

with open channels increases the filtration surface area and decreases the flux decline [73]. Small pellets shown in the images probably come from the manufacturing process of the membrane and can be easily distinguished from the MPs profiles.

Besides showing great MPs removal and good performance for long-term system applications [56], cellulose acetate has a promising future perspective. It is an eco-friendly bio-based polymer obtained from cellulose through acetylation of some of the hydroxyl groups. It might take up to 10 years to decompose, but unlike typical synthetic plastics, it can break down in the natural environment with no adverse impacts. Nevertheless, the bio-decomposition strongly depends on the environmental conditions, temperature, moisture level, and the degree of acetyl substitution [74,75].

Bio-degradability of cellulose acetate is an advantage on the one hand, as contamination from the membrane embrittlement does not contribute to further pollution. However, on the other hand, physical and chemical cleaning need extra attention as they could speed up the degradation of the membrane material and the possibility of breakage, favouring the releasing of micro- and nanoplastics, the so-called secondary pollution of MPs [76,77]. Also, cleaning procedures might increase the dimensions of the membrane's pore size through the mechanical stresses and physical flushing, while chemical cleaning might introduce by-products that can be adsorbed on the hydrophobic surface of the MPs before being released, increasing their hazard [77].

3.1.4. Other characterization

For a later discussion, it is essential to consider the values of the zeta potential of the MPs particles and the membrane. At neutral pH, PA's zeta potential crossed the 0 mV, therefore, showing a high degree of aggregation, while PS particles displayed a slightly negative potential with a magnitude of 20 mV and a slightly negative surface charge [56]. Finally, CA microfiltration membrane's zeta potential was reported to be -35 ± 1 mV at pH 6 and -45 ± 1 at pH 8 [78].

The microplastics formed dispersed colloidal suspensions in water due to their small size and water-like density, 1.13 g/cm^3 for PA and 1.05 g/cm^3 for PS, as reported in their manufacture datasheets. Yet, as described by their low zeta potential value, the suspensions were unstable over time, and the particles were partially settling at the bottom or on the water's surface, but with some particles fluctuating halfway through the container even after 24 h (pictures of the suspensions are provided in Appendix C). We can conclude that using microfiltration instead of simple decantation to separate microplastics is an advantage considering a faster separation time and a higher removal efficiency. Furthermore, microfiltration only requires a small transmembrane pressure to drive the flow across the membrane; therefore, it does not involve high energy costs.

The water contact angle was attempted on a clean cellulose acetate membrane, but the drop was absorbed entirely as soon as it touched the surface, showing a high degree of hydrophilicity. Both the negative surface charge and the high hydrophilicity are good membrane properties to reduce fouling by MPs and increase the water flux allowed [79]. Repulsive polar forces are expected between the hydrophobic PA and PS particles and the hydrophilic membrane. Also, repulsive electrostatic forces could occur mainly among the PS particles and between the PS particles and the CA membrane surface. These factors will be further considered when discussing the fouling results.

Finally, profilometry analyses were performed. The roughness value of cellulose acetate was similar within the experimental error to other commercial membranes, such as polycarbonate and PTFE, with values respectively of 1.28 ± 0.31 μm versus 1.41 ± 0.18 μm and 1.69 ± 0.42 μm. The presence of highly roughed surfaces with irregularities and bumpiness would give an additional physical interaction between the MPs and the membrane. In general, higher roughness values induce a higher fouling rate, and the main processes implied are foulant-membrane interactions, steric effects, hydrodynamic conditions, and permeation flux [80]. However, the surface roughness role becomes dominant only when the particles' size and shape match the valley regions of the membrane.

3.2. Kinetic and mechanistic aspects of cellulose acetate membrane fouling by PA and PS particles

Filtrations of pure water through the membrane up to 1 bar were first performed as a control experiment. No changes in the flow were noticed after 1 h of experimental run and during overnight recirculation. Therefore, contrary to ultrafiltration membranes, the CA membrane under study did not need to be compacted to ensure the stability of the permeate water flux. The flux stability after distilled water filtration can be found in Supporting Information, Appendix D.

The first objective was to identify the successive prevailing mechanisms occurring during the filtration runs. From the flow meter data set, $V(t)$ was evaluated. According to Grenier et al. [59], post-processing methods have been used to attenuate the noise of the experimental data and the finite difference method to derive the parameters d^2t/dV^2 and dt/dV. Finally, n was evaluated to identify the main controlling fouling mechanisms as described in Eq. (3), while the kinetic constants were assessed by the corresponding equations in Table 1.

Fig. 6b only shows some selected experimental values to highlight the main trend and facilitate the identification of the n-mechanism, which is shown in the graph. We can draw in conclusion that the leading mechanisms of the filtration run are complete pore blocking (corresponding to $n \approx 2$) followed by cake formation ($n \approx 0$). The intermediate pore blocking is probably obscured by the effect of complete pore coverage, which is then followed by the deposition of other particles on top of the membrane surface to form the cake layer. This agrees with the mentioned case where $d_{pore} \leq d_{particle}$. Since the case $d_{pore} << d_{particle}$ could also represent our conditions, comparison studies with only cake formation as the controlling mechanism were also performed. Fig. 7 represents the experimental data by fitting "model 1", only cake formation considered through the entire run, or "model 2", the combination of complete pore blocking followed by cake formation. The experimental curves shown correspond to the averaged value when 10 mg/L at 0.3 bar of MPs are filtered. In both cases, "model 2" fitted the data better and led to a higher coefficient of determination, R^2. The difference between the models is more pronounced when higher fouling occurs in both cases.

The filtrations with various feed MPs dosage and different operating TMP were evaluated to find the corresponding fouling characteristics. K_b and K_c were assessed by fitting the equations in Table 1 and by minimising the sum of squared errors (SSEs) between the predicted and experimental curves (Microsoft Excel Solver). Finally, an extra equation was added to ensure continuity passing from one mechanism to the other. At least five replicates for each condition were obtained to evaluate the averaged values and the standard deviation errors.
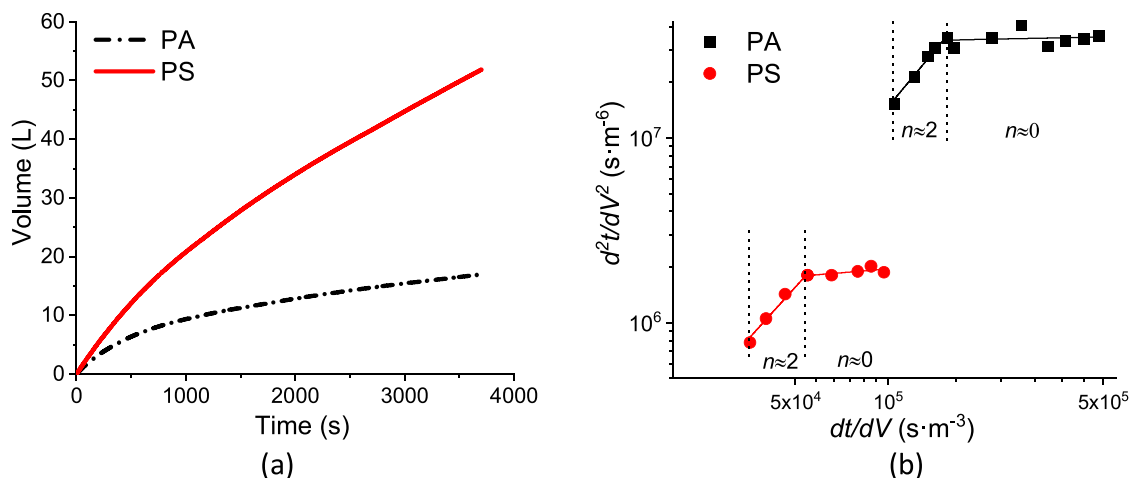
3.2.1. Varying MPs load

Fig. 8 shows the permeate flux decline during constant pressure filtrations at different MPs load. The experimental curves were then fitted with the two-model giving satisfactory results ($R^2 > 0.98$), Appendix E.

Fig. 9 and Fig. 10 show the correlation between the kinetic constants with the suspension MPs type and dosage in water. Since η_B is a function of the initial flux, it was reported. On the other hand, since η_C is a function of two constants, TMP fixed at 0.3 bar and the fluid viscosity, the pattern is the same as K_c and, therefore, not reported.

The blocking parameter η_B, chosen for discussion since it takes into account the initial flux, and the kinetic constant K_c are strongly correlated with the MPs load through a power-law relation. In particular, a stronger correlation was found in the case of PS, where fouling depends on $C^{\sim 2.3}$, while for PA on $C^{\sim 1.4}$. PS-induced fouling did not change much at low dosages, from 1 to 5 mg/L, but increased critically at higher MPs load. On the other hand, PA-induced fouling showed noticeable differences at low dosages and increased less critically than PS at higher dosages. The power-law relationship can be explained by the rise in steric obstacles at the pore entrance and by an increase in the interactions that occur in the presence of a greater amount of particles. This also explains the higher dependence on MPs load in the case of PS particles since averaged d_{PS} was greater than d_{PA}.

Besides the trend, both η_B and K_c show a higher value after PA filtration than PS, signifying higher fouling in the first case. This is an indicator of the interaction occurring among the MPs particles and between the MPs and the membrane. A denser cake layer was formed among the PA particles, probably due to the hydrophobic interaction. In contrast, when particles are charged, like in the case of PS particles, intermolecular repulsion between the particles and the membrane, both negatively charged, could increase the cake layer's porosity and avoid forming a thick and compact layer. The cake aspect after PA and PS filtrations is shown in Fig. 11.

In the first case, the cake layer was united and compacted on the membrane, while in the second case, the particles tended to leave the membrane more easily. Also, particle size distribution and particle shape appear to play an important role. Li et al., in two previous studies [52, 81], reported higher fouling by MPs in the range of 1.0–2.7 μm instead of smaller and larger sizes, explained by the formation of a more dense layer due to their binder action. Finally, it was reported that non-spherical particles induce less fouling since a looser cake layer can be formed due to the varied particles' orientations [54]. Therefore the smaller particle size distribution of PA particles could have contributed to the compactness of the cake layer, while the irregular shapes have helped its looseness. The sharp-cornered PS particles coming from cryogenic milling could have also caused membrane abrasion, later

Fig. 6. Plot of cumulative permeate volume V (L) versus time(s) for PA in black dash-dotted line and PS in red straight line (a). Plot of d^2t/dV^2 versus dt/dV for the determination of n, black squares for PA and red dots for PS (b). Both curves refer to a representative curve at 10 mg/L and 0.3 bar.
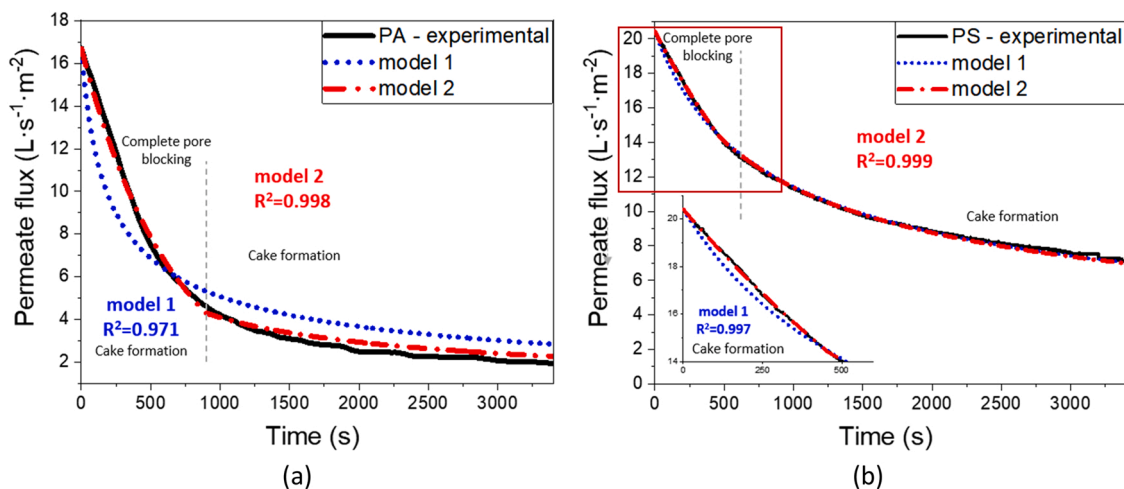
Fig. 7. Comparison between model 1 (when only cake formation occurs) and model 2 (complete pore blocking followed by cake formation). The experimental curve represents the averaged value for PA filtrations (a) and PS filtration at 10 mg/L and 0.3 bar.

Fig. 8. Permeate flux decline after 1 h of PA (a) and PS (b) filtrations at different MPs loads. The solid line corresponds to the average of the replicates, while the colour band around it indicates the error experienced under that operating condition.

Fig. 9. Kinetic constant for complete pore blocking (a) and the blocked surface area parameter (b) for PA (black squares) and PS (red dots) at variable MPs load, both reported on the same scale.
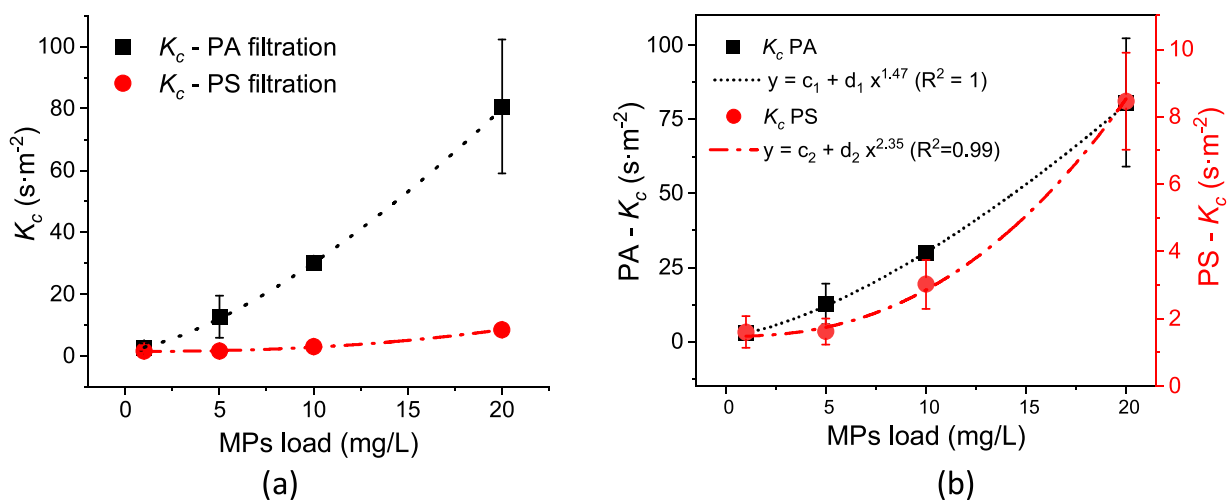
Fig. 10. Kinetic constant for cake formation as a function of MPs load for PA (black squares) and PS (red dots) in the same scale (a) and a magnification of the two trends on two scales (b).
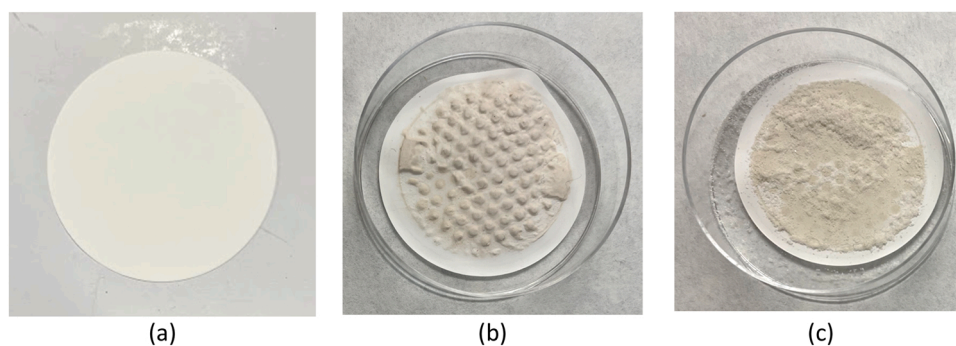
Fig. 11. Camera images of the pristine membrane (a) and after filtration with PA (b) and PS (c).

confirmed by the SEM images shown in Fig. 16, leading to bigger pore size diameters and higher membrane porosity, which let more flux pass through. The major interactions occurring at the interface MPs-CA membrane are summarised in Appendix F.

3.2.2. Varying TMP working pressure

Fig. 12 shows the permeate flux decline at different transmembrane working pressure which was kept constant during the entire filtration.

While Fig. 13a and Fig. 14a show the correlation between the kinetic constants with the MPs type and the working TMP, and Table S2 (Appendix E) lists all the fitting values for the two-model ($R^2 > 0.98$). This time, η_C is also reported since it depends on the pressure drop according to Eq. (13), therefore showing a different pattern compared to K_c.

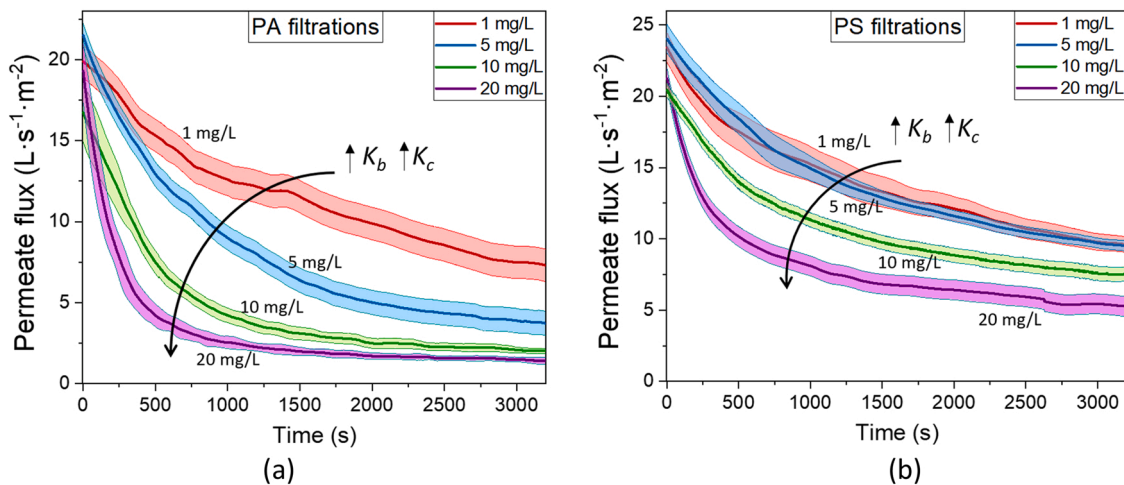By increasing the TMP, the K_c values decrease until reaching a

Fig. 12. Permeate flux decline after 1 h of PA (a) and PS (b) filtrations at different working TMP. The solid line corresponds to the average of the replicates, while the colour band around it indicates the error experienced under that operating condition.
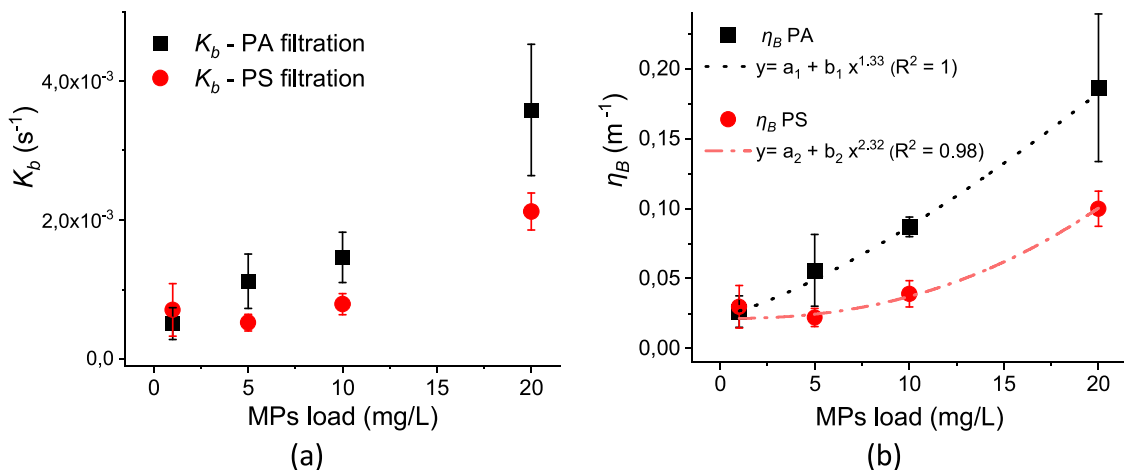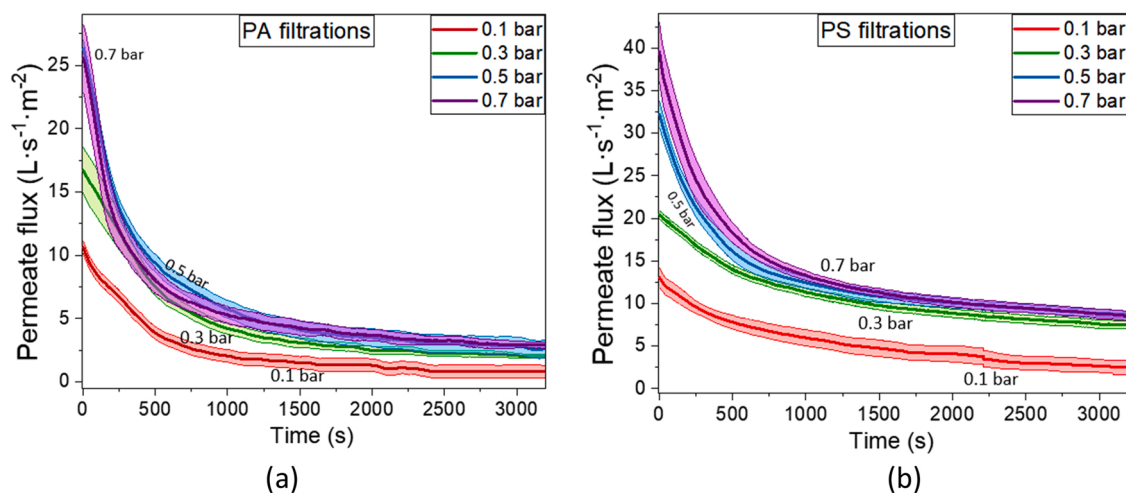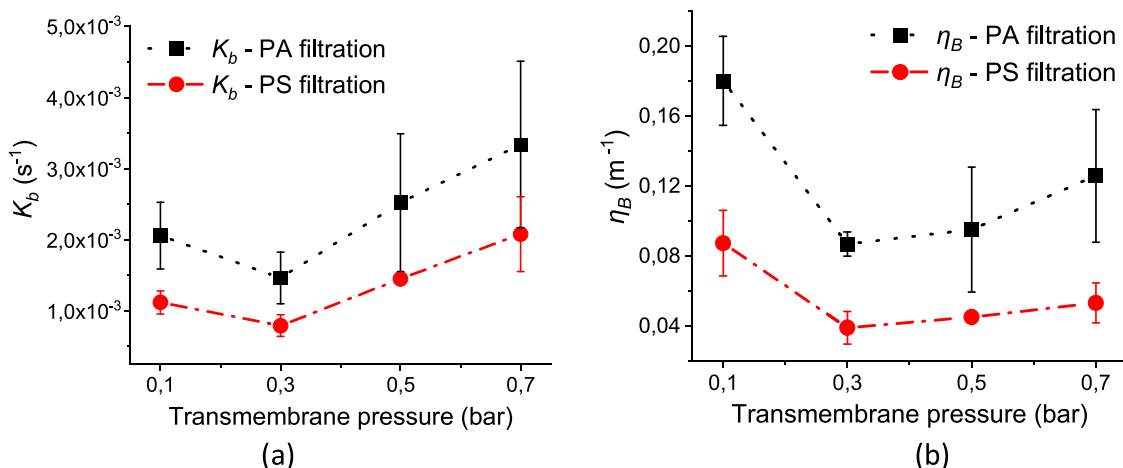
Fig. 13. Kinetic constant for complete pore blocking (a) and the blocked surface area parameter (b) for PA (black squares) and PS (red dots) as a function of transmembrane pressures, represented on the same scale.
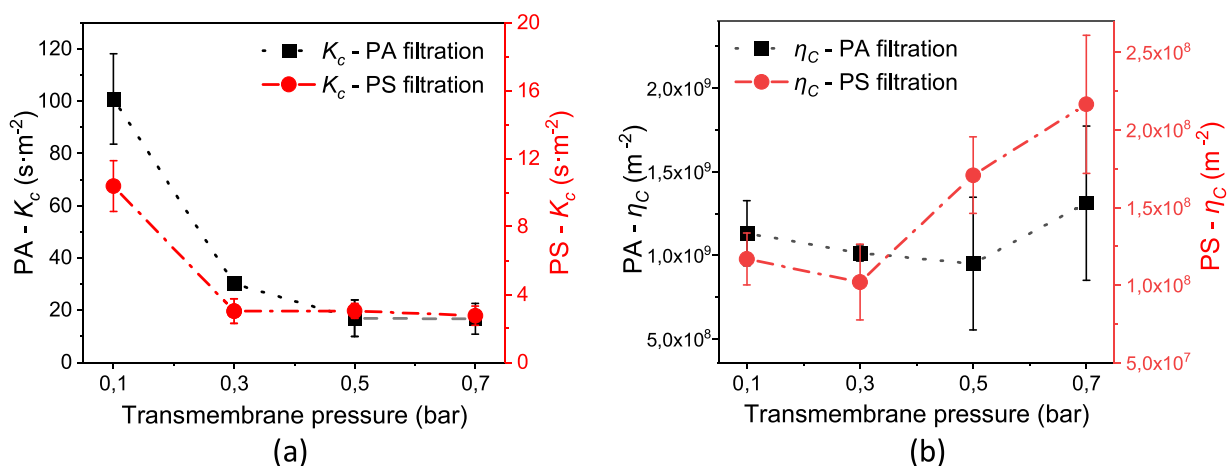

Fig. 14. Kinetic constant for cake filtration (a) and cake volumic specific resistance (b) for PA (black squares) and PS (red dots) as a function of transmembrane pressures, represented on two different scales to appreciate the trends.

constant value, within the experimental error, at a threshold pressure corresponding to a value between 0.3 and 0.5 bar for PA and 0.3 bar for PS filtration. Similarly, K_b, η_C, and η_B show a minimum in correspondence of the same TMP value (Fig. 13 and Fig. 14b).

At lower pressures, the particles have a higher tendency to stick on the membrane, but once the pressure reaches the threshold pressure value, the shear stress at the pore entrance is able to lift the particles captured at the membrane surface pore or part of the cake layer, freeing some blocked pores and decreasing the cake's density, with a result of a weaker fouling [65]. The shear stress is an important factor in membrane fouling. It affects it through the three main resistances: $R_{m,0}$, $R_{m,B}$, and R_C, and it is mathematically related to the lift force that can shift the particle away from the membrane surface [82]. It is often manipulated to control and alleviate membrane fouling, although the foulant properties play an important role in this potential mitigation. Li et. al [52] have proved in their work that applying rotation or helical rotation to increase the wall shear stresses is an effective fouling alleviator for PS particles. Alternatively, Enfrin et al. [83,84] showed the effectiveness of periodic gas scouring to generate higher shear forces with gas bubbles and reduce the fouling by PE micro- and nanoparticles, and PET nanofibers on hydrophobic PSF membranes.

Nevertheless, working at higher TMP and higher shear stresses is also not optimal as it would increase the operational costs and the energy consumption without further advantages for the membrane fouling. In

theory, for "rigid" foulants, the stronger the shear stress, the weaker the fouling [82]; however, MPs cannot be considered "rigid" particles since they can be affected by the mechanical impacts during the filtration run [85]. An increase in TMP probably leads to a higher membrane abrasion mechanism and particles' breakup [56]. The former leads to larger membrane pores and a reduction in MPs removal. The second leads to higher contamination of NPs considered more hazardous and could also cause more severe fouling, acting as a binder in the cake layer due to their interstitial effects [82,86].

The best working conditions are then represented by the threshold pressure value where the kinetic constants are at their minimum or

Table 3
Wall shear stress values for the two microplastic types at the beginning of the filtration ($\tau_{w,0}$) and between the transition from complete pore blocking to cake formation ($\tau_{w,b->c}$).

MP type	ΔP (bar)	J_0 (L s^{-1} m^{-2})	$J_{b\to c}$ (L s^{-1} m^{-2})	$\tau_{w,0}$ (Pa)	$\tau_{w,b\to c}$ (Pa)
PA	0.1	11.35	2.67	16.16	3.81
PA	0.3	16.72	4.32	23.81	6.15
PA	0.5	26.33	7.91	37.50	11.26
PA	0.7	25.97	9.47	36.98	13.49
PS	0.1	13.06	8.35	18.60	11.88
PS	0.3	20.42	13.62	29.08	19.39
PS	0.5	32.20	18.34	45.85	26.11
PS	0.7	39.55	21.54	56.32	30.67

reach a constant value.

Table 3 shows the wall shear stresses, τ_w, calculated following Eq. (14), occurring during the filtration at the beginning of complete pore blocking, $\tau_{w,0}$, and at the transition from complete pore blocking to cake formation $\tau_{w,b\to c}$.

$$\tau_w = -\mu \frac{du}{dr}\bigg|_{r=R} = 4\mu \frac{\overline{u}}{R} = 8\mu \frac{\overline{u}}{d_{pore}} \tag{14}$$

Where u is the flux velocity and r is the radius of the membrane pore. The complete table of the calculations with the standard deviations can be found in Appendix G of the Supplementary Information.

From Table 3, J_0 at 0.7 bar for PA filtration is curiously similar to the value at 0.5 bar. This can be explained as at the time the pressure was reaching 0.7 bar, the high fouling rate was already lowering the flux allowed to pass through the membrane.

Since higher flux rises, the shear stress values are generally higher for PS particles than PA particles. Also, the difference between the shear stresses at lower pressures is greater when comparing the values at the transition of the mechanisms compared to the beginning of filtration. This explains why, similarly to the kinetics at different MPs load, K_b and η_B could be represented on the same scale, while K_c and η_C values differed by one order of magnitude between the two MPs and therefore represented on two scales, indicating that cake formation is the mechanism more influenced by the particle type suspension.

3.3. Impact of PA and PS fouling on membrane surface properties

Water contact angle and profilometry analysis were also conducted after the MPs filtration to study changes on the membrane surface properties during the fouling. In the case of a pristine CA membrane, the water drop was spreading at the moment of the contact (complete wetting), while after PA and PS filtration, the water contact angle was greater than 90° but below 180°, indicating incomplete wetting, where the shape of the drop was spherical on top of the MPs cake layer. As shown in Fig. 15, also profilometry significantly increased after 1 h, and in particular, a higher increase was noticed for PA particles where higher fouling also occurred. An increase in hydrophobicity and roughness of the fouled membrane surface over time may have contributed to further fouling, increasing MPs-membrane surface interactions. The sites where big PS particles were part of the cake layer were not considered for the final roughness value since they were only creating a local roughness much higher than the representative value (see Appendix H).

Finally, SEM images were also taken after the filtrations to study the potential abrasion of the CA membrane surface due to the regular-shaped PA particles versus the irregular-shaped PS particles (Fig. 16). In this case, Fig. 16a and c have the same magnification of 1000x, while Fig. 16b and d have slightly different magnifications to best represent

the cross-section, 600x and 500x, respectively. In the case of PS filtration, the thin selective layer of the native membrane is destroyed by the sharp-cornered particles, reducing the selective blockage of the particles above the membrane nominal pore size. The abrasion occurred to a much lower degree after PA particles filtration, where the selective layer can still be easily identified through all the images. Therefore, we can conclude that the occurrence of membrane abrasion is not negligible when highly irregular and spiky particles are filtered. Nevertheless, cross-section images revealed some trapped MPs in the porous structure of the membrane in both cases. Finally, we can also assume that the limited roughness of the membrane alone did not create ridges and valleys for the capture of the particles, while those of the cake layer potentially created good spaces for the other particles to sit in.

In Supplementary Information (Appendix H), more SEM images of the membrane alone and after the fouling are reported.

On the one hand, backwash and other physical and chemical cleaning processes are a good solution to reduce fouling; however, they dilute and reintroduce the MPs back into the water, not reducing the overall problem. Furthermore, together with chemical agents, they could lead to further abrasion of the membrane or its weakening, causing a subsequent release of the MPs/NPs into the water. For example, LaRue et al. [52] reported that the backwashed membrane showed visible cracks in the cake layer and could have also cracked the membrane underneath. Therefore, direct replacement should be considered when the membrane is cheap, available, and does not cause further environmental pollution. MPs could then be recovered, recycled and reused for further purposes. For instance, they could be re-heated and extruded into new garments yarn or degraded into carbon dioxide and water for carbon extraction [87]. Nevertheless, replacement might be feasible only in households or small drinking water treatment plants, where the treated water alone does not create excessive fouling and, therefore, the membrane does not need to be replaced very often. Considering a more realistic scenario of the membrane working time, every hour of 10 mg/L of MPs filtration corresponds to approximately 42 days of operation in the case of water contaminated with 10 μg/L (see Appendix I).

4. Conclusions

In this study, the fouling induced by MPs on a commercial CA membrane in dead-end microfiltration configuration was investigated. According to the sequential modelling results for permeate flux decline at constant pressure, the main mechanisms occurring were complete pore blocking followed by cake layer formation, with a good agreement between the models and the experimental data. The corresponding mechanisms' kinetic constants were studied for two types of MPs, polyamide and polystyrene, and at different operating conditions, varying MPs load and operating TMP. As a result:
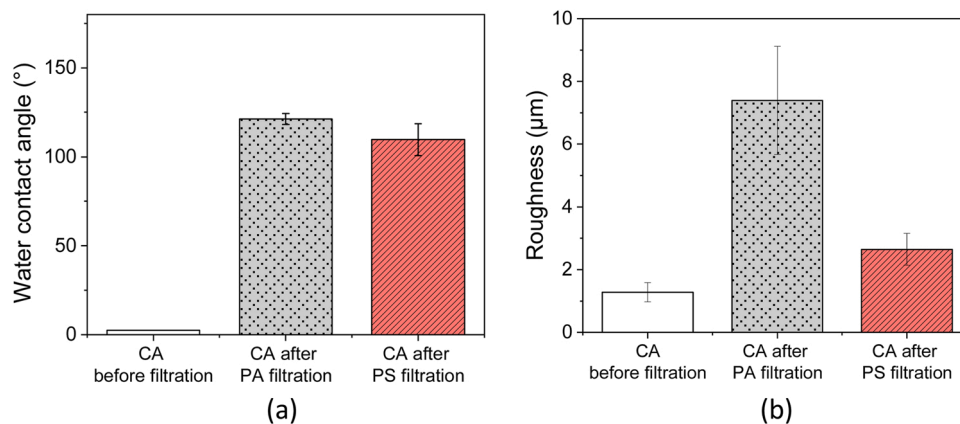

Fig. 15. Water contact angle (a) and profilometry (b) measured before and after the filtration of MPs (10 mg/L at 0.3 bar).
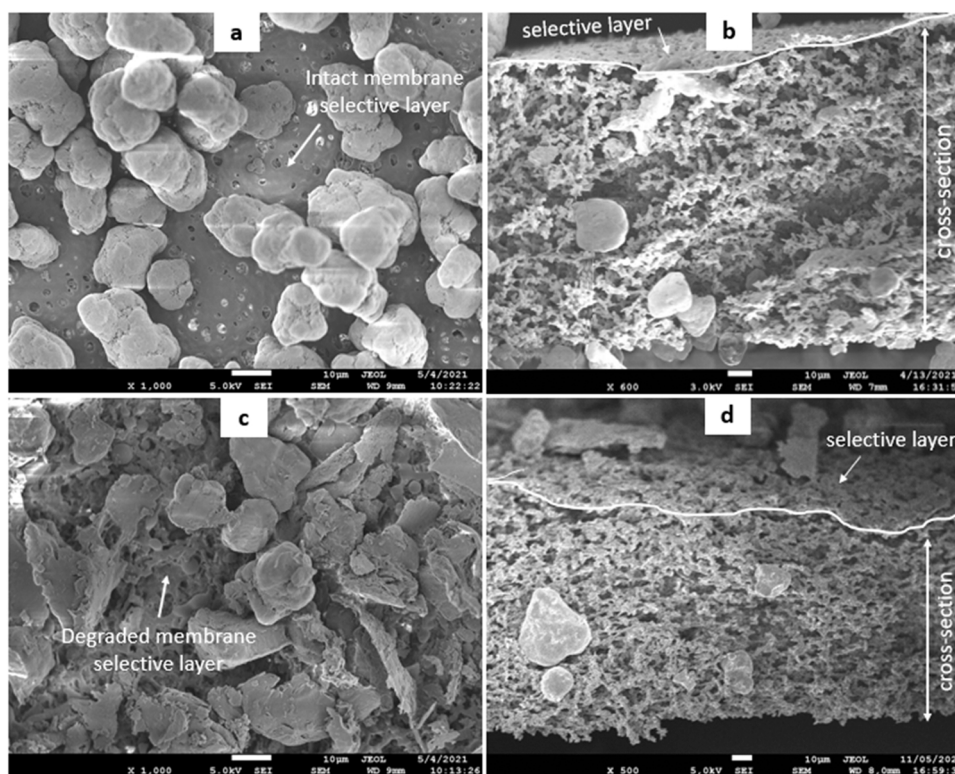
Fig. 16. SEM images of the membrane surface (a and c after PA and PS filtration) and cross-section (b and d after PA and PS filtration). All images display a unit distance of 10 μm.

- Increasing MPs load led to an increase in the kinetic constants. Both K_c and η_B followed a similar power-law relationship depending on $C^{\sim 2.3}$ for PS and $C^{\sim 1.4}$ for PA particles. A stronger correlation was found in the case of PS, which can be addressed to the greater particles' dimensions that created more steric hindrance interactions compared to PA.
- Increasing the working TMP led to a threshold pressure value identified as the best working condition, which is the right compromise between lowering the fouling and avoiding increasing the operational costs, other than limiting particles breakage and membrane abrasion. The best conditions were found to be between 0.3 and 0.5 bar for PA and 0.3 bar for PS particles.
- Higher fouling occurred after PA filtration, which can be addressed to the higher PA hydrophobicity and their particles' neutral charge, together with the smaller particles' size, which could interlay and act as a binder during the cake formation, causing a denser layer. On the other hand, the repulsive electrostatic interactions among the PS particles and the negatively charged CA membrane, together with the high shape irregularity of the particles, formed a looser cake layer and induced greater abrasion on the CA surface, visibly reducing the selective layer and allowing more flux to pass through. Finally, the increase in hydrophobicity and roughness of the fouled membrane surface may have contributed to further fouling.

To avoid secondary MPs pollution and their reintroduction in water streams, an alternative to physical and cleaning procedures in households or small drinking water treatments could be the direct replacement when fouling is unmaintainable, also allowing the recovery and the recycling of the particles. Hence, modelling membrane fouling can help foresee the best working conditions with the specific foulant present in the water to be treated and predict the membrane replacement cycles to increase the MPs removal efficiency.

CRediT authorship contribution statement

A.R.P. Pizzichetti: Conceptualization, Methodology, Investigation, Data curation, Visualisation, Writing – original draft, Writing – review & editing. **C. Pablos:** Supervision, Methodology, Writing – review & editing, Funding acquisition. **C. Álvarez-Fernández:** Investigation, Writing – review. **K. Reynolds:** Supervision, Writing – review & editing, Funding acquisition. **S. Stanley:** Supervision, Writing – review, Funding acquisition. **J Marugán:** Supervision, Methodology, Writing – review & editing, Funding acquisition.

Declaration of Competing Interest

The authors declare that they have no known competing financial interests or personal relationships that could have appeared to influence the work reported in this paper.

Data Availability

The authors have included the link to the data in the attached documents.

Appendix A. Supporting information

Supplementary data associated with this article can be found in the online version at doi:10.1016/j.jece.2023.109338.

References

[1] A. Gogoi, P. Mazumder, V.K. Tyagi, G.G. Tushara Chaminda, A.K. An, M. Kumar, Occurrence and fate of emerging contaminants in water environment: a review, Groundw. Sustain. Dev. 6 (2018) 169–180, https://doi.org/10.1016/j.gsd.2017.12.009.

[2] B.S. Rathi, P.S. Kumar, P.L. Show, A review on effective removal of emerging contaminants from aquatic systems: current trends and scope for further research, J. Hazard. Mater. 409 (2021), 124413, https://doi.org/10.1016/j.jhazmat.2020.124413.

[3] J. Li, H. Liu, J. Paul Chen, Microplastics in freshwater systems: a review on occurrence, environmental effects, and methods for microplastics detection, Water Res. 137 (2018) 362–374, https://doi.org/10.1016/j.watres.2017.12.056.

[4] Association of Plastic Manufacturers, Plastics – the Facts 2020, PlasticEurope. (2020). ⟨https://plasticseurope.org/wp-content/uploads/2021/09/Plastics_the_facts-WEB-2020_versionJun21_final.pdf⟩ (accessed April 1, 2022).

[5] R. Geyer, J.R. Jambeck, K.L. Law, Production, use, and fate of all plastics ever made, Sci. Adv. 3 (2017), https://doi.org/10.1126/SCIADV.1700782.

[6] A. Chamas, H. Moon, J. Zheng, Y. Qiu, T. Tabassum, J.H. Jang, M. Abu-Omar, S. L. Scott, S. Suh, Degradation rates of plastics in the environment, ACS Sustain. Chem. Eng. 8 (2020) 3494–3511, https://doi.org/10.1021/ACSSUSCHEMENG.9B06635.

[7] J. Sun, X. Dai, Q. Wang, M.C.M. van Loosdrecht, B.J. Ni, Microplastics in wastewater treatment plants: detection, occurrence and removal, Water Res. 152 (2019) 21–37, https://doi.org/10.1016/j.watres.2018.12.050.

[8] W.C. Li, H.F. Tse, L. Fok, Plastic waste in the marine environment: a review of sources, occurrence and effects, Sci. Total Environ. 566–567 (2016) 333–349, https://doi.org/10.1016/j.scitotenv.2016.05.084.

[9] P. Kay, R. Hiscoe, I. Moberley, L. Bajic, N. McKenna, Wastewater treatment plants as a source of microplastics in river catchments, Environ. Sci. Pollut. Res. 25 (2018) 20264–20267, https://doi.org/10.1007/s11356-018-2070-7.

[10] L. Peng, D. Fu, H. Qi, C.Q. Lan, H. Yu, C. Ge, Micro- and nano-plastics in marine environment: source, distribution and threats — a review, Sci. Total Environ. 698 (2020), 134254, https://doi.org/10.1016/j.scitotenv.2019.134254.

[11] L.M. Rios Mendoza, H. Karapanagioti, N.R. Álvarez, Micro(nanoplastics) in the marine environment: current knowledge and gaps, Curr. Opin. Environ. Sci. Heal 1 (2018) 47–51, https://doi.org/10.1016/j.coesh.2017.11.004.

[12] S.C. Gall, R.C. Thompson, The impact of debris on marine life, Mar. Pollut. Bull. 92 (2015) 170–179, https://doi.org/10.1016/j.marpolbul.2014.12.041.

[13] F. Ribeiro, J.W. O'Brien, T. Galloway, K.V. Thomas, Accumulation and fate of nano- and micro-plastics and associated contaminants in organisms, TrAC - Trends Anal. Chem. 111 (2019) 139–147, https://doi.org/10.1016/j.trac.2018.12.010.

[14] K. Gunaalan, E. Fabbri, M. Capolupo, The hidden threat of plastic leachates: a critical review on their impacts on aquatic organisms, Water Res. 184 (2020), 116170, https://doi.org/10.1016/j.watres.2020.116170.

[15] F. Wang, C.S. Wong, D. Chen, X. Lu, F. Wang, E.Y. Zeng, Interaction of toxic chemicals with microplastics: a critical review, Water Res. 139 (2018) 208–219, https://doi.org/10.1016/j.watres.2018.04.003.

[16] S. Lambert, M. Wagner. Freshwater Microplastics, Springer, 2018, https://doi.org/10.1007/978-3-319-61615-5.

[17] O.H. Fred-Ahmadu, G. Bhagwat, I. Oluyoye, N.U. Benson, O.O. Ayejuyo, T. Palanisami, Interaction of chemical contaminants with microplastics: Principles and perspectives, Sci. Total Environ. 706 (2020), 135978, https://doi.org/10.1016/j.scitotenv.2019.135978.

[18] L.M. Santos, S. Rodríguez-Mozaz, D. Barceló, Microplastics as vectors of pharmaceuticals in aquatic organisms – an overview of their environmental implications, Case Stud. Chem. Environ. Eng. 3 (2021) 100079, https://doi.org/10.1016/j.cscee.2021.100079.

[19] T. Atugoda, H. Wijesekara, D.R.I.B. Werellagama, K.B.S.N. Jinadasa, N.S. Bolan, M. Vithanage, Adsorptive interaction of antibiotic ciprofloxacin on polyethylene microplastics: Implications for vector transport in water, Environ. Technol. Innov. 19 (2020), 100971, https://doi.org/10.1016/j.eti.2020.100971.

[20] E.R. Zettler, T.J. Mincer, L.A. Amaral-Zettler, Life in the "plastisphere": microbial communities on plastic marine debris, Environ. Sci. Technol. 47 (2013) 7137–7146, https://doi.org/10.1021/es401288x.

[21] Q. Zhang, E.G. Xu, J. Li, Q. Chen, L. Ma, E.Y. Zeng, H. Shi, A review of microplastics in table salt, drinking water, and air: direct human exposure, Environ. Sci. Technol. 54 (2020) 3740–3751, https://doi.org/10.1021/acs.est.9b04535.

[22] D. Santillo, K. Miller, P. Johnston, Microplastics as contaminants in commercially important seafood species, Integr. Environ. Assess. Manag. 13 (2017) 516–521, https://doi.org/10.1002/ieam.1909.

[23] M. Revel, A. Châtel, C. Mouneyrac, Micro(nano)plastics: a threat to human health, Curr. Opin. Environ. Sci. Heal 1 (2018) 17–23, https://doi.org/10.1016/j.coesh.2017.10.003.

[24] K. Novotna, L. Cermakova, L. Pivokonska, T. Cajthaml, M. Pivokonsky, Microplastics in drinking water treatment – current knowledge and research needs, Sci. Total Environ. 667 (2019) 730–740, https://doi.org/10.1016/j.scitotenv.2019.02.431.

[25] Y. Picó, D. Barceló, Analysis and prevention of microplastics pollution in water: current perspectives and future directions, ACS Omega 4 (2019) 6709–6719, https://doi.org/10.1021/acsomega.9b00222.

[26] D. Barcelo, Y. Pico, Case studies of macro- and microplastics pollution in coastal waters and rivers: is there a solution with new removal technologies and policy actions, Case Stud. Chem. Environ. Eng. (2020), 100019, https://doi.org/10.1016/j.cscee.2020.100019.

[27] M. Shen, B. Song, Y. Zhu, G. Zeng, Y. Zhang, Y. Yang, X. Wen, M. Chen, H. Yi, Removal of microplastics via drinking water treatment: current knowledge and future directions, Chemosphere 251 (2020), 126612, https://doi.org/10.1016/j.chemosphere.2020.126612.

[28] O.M. Rodríguez-Narvaez, A. Goonetilleke, L. Perez, E.R. Bandala, Engineered technologies for the separation and degradation of microplastics in water: a review, Chem. Eng. J. 414 (2021), 128692, https://doi.org/10.1016/j.cej.2021.128692.

[29] A. Kundu, N.P. Shetti, S. Basu, K. Raghava Reddy, M.N. Nadagouda, T. M. Aminabhavi, Identification and removal of micro- and nano-plastics: efficient and cost-effective methods, Chem. Eng. J. 421 (2021), 129816, https://doi.org/10.1016/J.CEJ.2021.129816.

[30] M.N. Nguyen, L.H. Nguyen, X.P. Nguyen, T.H. Le, V. Viet, A techno-environmental assessment from microplastic characterization to its removal by innovative technologies, J. Mech. Eng. Res. Dev. 44 (2021) 55–68.

[31] Y. Zhang, H. Jiang, K. Bian, H. Wang, C. Wang, A critical review of control and removal strategies for microplastics from aquatic environments, J. Environ. Chem. Eng. 9 (2021) 105463, https://doi.org/10.1016/J.JECE.2021.105463.

[32] I. Ali, T. Ding, C. Peng, I. Naz, H. Sun, J. Li, J. Liu, Micro- and nanoplastics in wastewater treatment plants: occurrence, removal, fate, impacts and remediation technologies – a critical review, Chem. Eng. J. 423 (2021), 130205, https://doi.org/10.1016/j.cej.2021.130205.

[33] M.R. Karimi Estahbanati, M. Kiendrebeogo, A. Khosravanipour Mostafazadeh, P. Drogui, R.D. Tyagi, Treatment processes for microplastics and nanoplastics in waters: state-of-the-art review, Mar. Pollut. Bull. 168 (2021), 112374, https://doi.org/10.1016/j.marpolbul.2021.112374.

[34] W. Perren, A. Wojtasik, Q. Cai, Removal of microbeads from wastewater using electrocoagulation, ACS Omega 3 (2018) 3357–3364, https://doi.org/10.1021/acsomega.7b02037.

[35] J. Grbic, B. Nguyen, E. Guo, J.B. You, D. Sinton, C.M. Rochman, Magnetic extraction of microplastics from environmental samples, Environ. Sci. Technol. Lett. 6 (2019) 68–72, https://doi.org/10.1021/acs.estlett.8b00671.

[36] Y. Tang, S. Zhang, Y. Su, D. Wu, Y. Zhao, B. Xie, Removal of microplastics from aqueous solutions by magnetic carbon nanotubes, Chem. Eng. J. 406 (2021), 126804, https://doi.org/10.1016/j.cej.2020.126804.

[37] S. Felsing, C. Kochleus, S. Buchinger, N. Brennholt, F. Stock, G. Reifferscheid, A new approach in separating microplastics from environmental samples based on their electrostatic behavior, Environ. Pollut. 234 (2018) 20–28, https://doi.org/10.1016/j.envpol.2017.11.013.

[38] C. Scherer, N. Brennholt, G. Reifferscheid, M. Wagner, Feeding type and development drive the ingestion of microplastics by freshwater invertebrates, Sci. Rep. 7 (2017) 1–9, https://doi.org/10.1038/s41598-017-17191-7.

[39] J. Gong, T. Kong, Y. Li, Q. Li, Z. Li, J. Zhang, Biodegradation of microplastic derived from Poly(ethylene terephthalate) with bacterial whole-cell biocatalysts, Polym Vol. 10 (2018) 1326, https://doi.org/10.3390/POLYM10121326.

[40] L. Cai, J. Wang, J. Peng, Z. Wu, X. Tan, Observation of the degradation of three types of plastic pellets exposed to UV irradiation in three different environments, Sci. Total Environ. 628– 629 (2018) 740–747, https://doi.org/10.1016/J.SCITOTENV.2018.02.079.

[41] P. Wang, Z. Huang, S. Chen, M. Jing, Z. Ge, J. Chen, S. Yang, J. Chen, Y. Fang, Sustainable removal of nano/microplastics in water by solar energy, Chem. Eng. J. 428 (2022), 131196, https://doi.org/10.1016/J.CEJ.2021.131196.

[42] Z. Wang, T. Lin, W. Chen, Occurrence and removal of microplastics in an advanced drinking water treatment plant (ADWTP), Sci. Total Environ. 700 (2020), 134520, https://doi.org/10.1016/j.scitotenv.2019.134520.

[43] R. Chen, M. Qi, G. Zhang, C. Yi, Comparative experiments on polymer degradation technique of produced water of polymer flooding oilfield, IOP Conf. Ser. Earth Environ. Sci. 113 (2018), 012208, https://doi.org/10.1088/1755-1315/113/1/012208.

[44] H. Hidayaturrahman, T.G. Lee, A study on characteristics of microplastic in wastewater of South Korea: identification, quantification, and fate of microplastics during treatment process, Mar. Pollut. Bull. 146 (2019) 696–702, https://doi.org/10.1016/J.MARPOLBUL.2019.06.071.

[45] H. Luo, Y. Zeng, Y. Zhao, Y. Xiang, Y. Li, X. Pan, Effects of advanced oxidation processes on leachates and properties of microplastics, J. Hazard. Mater. 413 (2021), https://doi.org/10.1016/j.jhazmat.2021.125342.

[46] B. Ma, W. Xue, C. Hu, H. Liu, J. Qu, L. Li, Characteristics of microplastic removal via coagulation and ultrafiltration during drinking water treatment, Chem. Eng. J. 359 (2019) 159–167, https://doi.org/10.1016/j.cej.2018.11.155.

[47] B. Ma, W. Xue, Y. Ding, C. Hu, H. Liu, J. Qu, Removal characteristics of microplastics by Fe-based coagulants during drinking water treatment, J. Environ. Sci. 78 (2019) 267–275, https://doi.org/10.1016/j.jes.2018.10.006.

[48] A.F. Herbort, M.T. Sturm, S. Fiedler, G. Abkai, K. Schuhen, Alkoxy-silyl induced agglomeration: a new approach for the sustainable removal of microplastic from aquatic systems, J. Polym. Environ. 26 (2018) 4258–4270, https://doi.org/10.1007/s10924-018-1287-3.

[49] A. Adewuyi, A.J. Campbell, O.G. Adeyemi, The potential role of membrane technology in the removal of microplastics from wastewater, J. Appl. Membr. Sci. Technol. 25 (2021) 31–53, https://doi.org/10.11113/amst.v25n2.216.

[50] T. Poerio, E. Piacentini, R. Mazzei, Membrane processes for microplastic removal, Molecules 24 (2019), https://doi.org/10.3390/MOLECULES24224148.

[51] M. Enfrin, J. Lee, P. Le-Clech, L.F. Dumée, Kinetic and mechanistic aspects of ultrafiltration membrane fouling by nano- and microplastics, J. Memb. Sci. 601 (2020), 117890, https://doi.org/10.1016/j.memsci.2020.117890.

[52] J. Li, B. Wang, Z. Chen, B. Ma, J.P. Chen, Ultrafiltration membrane fouling by microplastics with raw water: behaviors and alleviation methods, Chem. Eng. J. 410 (2021), 128174, https://doi.org/10.1016/j.cej.2020.128174.

[53] R.J. LaRue, B. Patterson, S. O'Brien, D.R. Latulippe, Evaluation of membrane fouling by microplastic particles in tertiary wastewater treatment processes, ACS Environ. Sci. Technol. Water 2 (2022) 955–966, https://doi.org/10.1021/acsestwater.1c00430.

[54] S. Sankaranarayanan, B. Likozar, R. Navia, Real-time particle size analysis using the focused beam reflectance measurement probe for in situ fabrication of polyacrylamide–filler composite materials, Sci. Rep. 9 (2019) 1–12, https://doi.org/10.1038/s41598-019-46451-x.

[55] L. Li, G. Xu, H. Yu, J. Xing, Dynamic membrane for micro-particle removal in wastewater treatment: performance and influencing factors, Sci. Total Environ. 627 (2018) 332–340, https://doi.org/10.1016/J.SCITOTENV.2018.01.239.

[56] A.R.P. Pizzichetti, C. Pablos, C. Álvarez-Fernández, K. Reynolds, S. Stanley, J. Marugán, Evaluation of membranes performance for microplastic removal in a simple and low-cost filtration system, Case Stud. Chem. Environ. Eng. 3 (2021), 100075, https://doi.org/10.1016/j.cscee.2020.100075.

[57] E. Iritani, N. Katagiri, Developments of blocking filtration model in membrane filtration, KONA Powder Part. J. 2016 (2016) 179–202, https://doi.org/10.14356/kona.2016024.

[58] J.A. Calles, J. Dufour, J. Marugán, J.L. Peña, R. Giménez-Aguirre, D. Merino-García, Properties of asphaltenes precipitated with different n -Alkanes. A study to assess the most representative species for modeling, Energy Fuels 22 (2008) 763–769, https://doi.org/10.1021/ef700404p.

[59] E.J. Hukkanen, R.D. Braatz, Measurement of particle size distribution in suspension polymerization using in situ laser backscattering, Sens. Actuators B Chem. 96 (2003) 451–459, https://doi.org/10.1016/S0925-4005(03)00600-2.

[60] K.J. Howe, M.M. Clark, Fouling of microfiltration and ultrafiltration membranes by natural waters, Environ. Sci. Technol. 36 (2002) 3571–3576, https://doi.org/10.1021/es025587r.

[61] E. Abbasi-Garravand, C.N. Mulligan, C.B. Laflamme, G. Clairet, Investigation of the fouling effect on a commercial semi-permeable membrane in the pressure retarded osmosis (PRO) process, Sep. Purif. Technol. 193 (2018) 81–90, https://doi.org/10.1016/j.seppur.2017.10.053.

[62] J. Hermia, Constant pressure blocking filtration laws: application to power-law non-newtonian fluids, Trans. Inst. Chem. Eng. 60 (1982) 183.

[63] R.W. Field, J.J. Wu, Modelling of permeability loss in membrane filtration: Re-examination of fundamental fouling equations and their link to critical flux, Desalination 283 (2011) 68–74, https://doi.org/10.1016/j.desal.2011.04.035.

[64] R.W. Field, D. Wu, J.A. Howell, B.B. Gupta, Critical flux concept for microfiltration fouling, J. Memb. Sci. 100 (1995) 259–272, https://doi.org/10.1016/0376-7388(94)00265-Z.

[65] A. Grenier, M. Meireles, P. Aimar, P. Carvin, Analysing flux decline in dead-end filtration, Chem. Eng. Res. Des. 86 (2008) 1281–1293, https://doi.org/10.1016/j.cherd.2008.06.005.

[66] T.A. Trinh, W. Li, J.W. Chew, Internal fouling during microfiltration with foulants of different surface charges, J. Memb. Sci. 602 (2020) 117983, https://doi.org/10.1016/j.memsci.2020.117983.

[67] C. Duclos-Orsello, W. Li, C.C. Ho, A three mechanism model to describe fouling of microfiltration membranes, J. Memb. Sci. 280 (2006) 856–866, https://doi.org/10.1016/j.memsci.2006.03.005.

[68] A.S. Tagg, M. Sapp, J.P. Harrison, J.J. Ojeda, Identification and quantification of microplastics in wastewater using focal plane array-based reflectance micro-FT-IR imaging, Anal. Chem. 87 (2015) 6032–6040, https://doi.org/10.1021/acs.analchem.5b00495.

[69] J.P. Harrison, J.J. Ojeda, M.E. Romero-González, The applicability of reflectance micro-Fourier-transform infrared spectroscopy for the detection of synthetic microplastics in marine sediments, Sci. Total Environ. 416 (2012) 455–463, https://doi.org/10.1016/j.scitotenv.2011.11.078.

[70] M.G.J. Löder, M. Kuczera, S. Mintenig, C. Lorenz, G. Gerdts, Focal plane array detector-based micro-Fourier-transform infrared imaging for the analysis of microplastics in environmental samples, Environ. Chem. 12 (2015) 563–581, https://doi.org/10.1071/EN14205.

[71] G. Renner, T.C. Schmidt, J. Schram, Characterization and Quantification of Microplastics by Infrared Spectroscopy, Elsevier Ltd, 2017, https://doi.org/10.1016/bs.coac.2016.10.006.

[72] H. Cai, E.G. Xu, F. Du, R. Li, J. Liu, H. Shi, Analysis of environmental nanoplastics: progress and challenges, Chem. Eng. J. 410 (2021), 128208, https://doi.org/10.1016/j.cej.2020.128208.

[73] M.G. Buonomenna, Design next generation membranes or rethink the "old" asymmetric membranes? Symmetry (Basel) 12 (2020) 10–13, https://doi.org/10.3390/sym12020270.

[74] N. Yadav, M. Hakkarainen, Degradable or not? Cellulose acetate as a model for complicated interplay between structure, environment and degradation, Chemosphere 265 (2021), 128731, https://doi.org/10.1016/J.CHEMOSPHERE.2020.128731.

[75] J. Puls, S.A. Wilson, D. Hölter, Degradation of cellulose acetate-based materials: a review, J. Polym. Environ. 19 (2011) 152–165, https://doi.org/10.1007/s10924-010-0258-0.

[76] M. Golgoli, M. Khiadani, A. Shafieian, T.K. Sen, Y. Hartanto, M.L. Johns, M. Zargar, Chemosphere microplastics fouling and interaction with polymeric membranes: a review, Chemosphere 283 (2021), 131185, https://doi.org/10.1016/j.chemosphere.2021.131185.

[77] H. Ding, J. Zhang, H. He, Y. Zhu, D.D. Dionysiou, Z. Liu, C. Zhao, Do membrane filtration systems in drinking water treatment plants release nano/microplastics, Sci. Total Environ. 755 (2021), 142658, https://doi.org/10.1016/J.SCITOTENV.2020.142658.

[78] S. Azari, L. Zou, E. Cornelissen, Y. Mukai, Facile fouling resistant surface modification of microfiltration cellulose acetate membranes by using amino acid L-DOPA, Water Sci. Technol. 68 (2013) 901–908, https://doi.org/10.2166/wst.2013.292.

[79] M. Enfrin, J. Wang, A. Merenda, L.F. Dum, J. Lee, Mitigation of membrane fouling by nano / microplastics via surface chemistry control, J. Memb. Sci. 633 (2021), 119379, https://doi.org/10.1016/j.memsci.2021.119379.

[80] C. Shang, D. Pranantyo, S. Zhang, Understanding the roughness-fouling relationship in reverse osmosis: mechanism and implications, Environ. Sci. Technol. 54 (2020) 5288–5296, https://doi.org/10.1021/acs.est.0c00535.

[81] Y.J. Liu, D.D. Sun, Particles size-associated membrane fouling in microfiltration of denitrifying granules supernatant, Chem. Eng. J. 181–182 (2012) 494–500, https://doi.org/10.1016/J.CEJ.2011.12.009.

[82] X. Du, Y. Wang, G. Leslie, G. Li, H. Liang, Shear stress in a pressure-driven membrane system and its impact on membrane fouling from a hydrodynamic condition perspective: a review, J. Chem. Technol. Biotechnol. 92 (2017) 463–478, https://doi.org/10.1002/jctb.5154.

[83] M. Enfrin, J. Lee, A.G. Fane, L.F. Dumée, Mitigation of membrane particulate fouling by nano / microplastics via physical cleaning strategies, Sci. Total Environ. 788 (2021), 147689, https://doi.org/10.1016/j.scitotenv.2021.147689.

[84] M. Enfrin, C. Hachemi, D.L. Callahan, J. Lee, L.F. Dumée, Membrane fouling by nanofibres and organic contaminants – mechanisms and mitigation via periodic cleaning strategies, Sep. Purif. Technol. 278 (2022), https://doi.org/10.1016/j.seppur.2021.119592.

[85] M. Enfrin, J. Lee, Y. Gibert, F. Basheer, L. Kong, L.F. Dumée, Release of hazardous nanoplastic contaminants due to microplastics fragmentation under shear stress forces, J. Hazard. Mater. 384 (2020), 121393, https://doi.org/10.1016/j.jhazmat.2019.121393.

[86] J. Kromkamp, F. Faber, K. Schroen, R. Boom, Effects of particle size segregation on crossflow microfiltration performance: control mechanism for concentration polarisation and particle fractionation, J. Memb. Sci. 268 (2006) 189–197, https://doi.org/10.1016/j.memsci.2005.06.012.

[87] T.K. Dey, M. Jamal, Separation of microplastics from water - What next? J. Water Process Eng. 44 (2021), 102332 https://doi.org/10.1016/j.jwpe.2021.102332.